Geochemical consequences of oxygen diffusion from the oceanic crust into overlying sediments and its significance for biogeochemical cycles based on sediments of the NE Pacific

Gerard J. M. Versteegh[1,2,3], Andrea Koschinsky[2,3], Thomas Kuhn[4], Inken Preuss[2*], Sabine Kasten[1,3,5]

5   [1]Alfred Wegener Institute, Helmholtz Centre for Polar and Marine Research, Bremerhaven, 27570, Germany
[2]Jacobs University Bremen, Department of Physics and Earth Sciences, Bremen, 28759, Germany
[3]MARUM – Zentrum für Marine Umweltwissenschaften, Universität Bremen, Bremen, 28359, Germany
[4]Bundesanstalt für Geowissenschaften und Rohstoffe. Hannover, 30655, Germany
[5]University of Bremen, Faculty of Geosciences, Bremen, 28359, Germany
10   *present address: GEOMAR Helmholtz Centre for Ocean Research, Kiel, 24148, Germany

Correspondence to: Gerard J. M. Versteegh (gerard.versteegh@awi.de)

Abstract. Exchange of dissolved substances at the sediment–water interface provides an important link between the short–term and long–term geochemical cycles in the ocean. A second, as yet poorly understood sediment–water exchange is supported by low–temperature circulation of seawater through the oceanic basement underneath the sediments. From the

15   basement, upwards diffusing oxygen and other dissolved species modify the sediment whereas reaction products diffuse from the sediment down into the basement, where they are transported by the basement fluid and released to the ocean. Here, we investigate the impact of this 'second' route with respect to transport, release and consumption of oxygen, nitrate, manganese, nickel, and cobalt on the basis of sediment cores retrieved from the Clarion Clipperton Zone (CCZ) in the equatorial Pacific Ocean. We show that in this abyssal ocean region characterised by low organic–carbon burial and

20   sedimentation rates vast areas exist where the downward and upward directed diffusive fluxes of oxygen meet so that the sediments are oxic throughout. This is especially the case where sediments are thin or in the proximity of faults. Oxygen diffusing upward from the basaltic crust into the sediment contributes to the degradation of sedimentary organic matter. Where the oxygen profiles do not meet, they are separated by a suboxic sediment interval characterised by Mn^{2+} in the pore–water. Where the sediments are entirely oxic, nitrate produced in the upper sediment by nitrification is lost both by upward

25   diffusion into the bottom water and by downward diffusion into the fluids circulating within the basement. Where pore–water manganese in the suboxic zones remains low, nitrate consumption is low and the sediment continues to deliver nitrate to the ocean bottom waters and basement fluid. We observe that at elevated pore–water manganese concentrations, nitrate consumption exceeds production and the basement becomes a nitrate source. Within the suboxic zone, not only manganese but also cobalt and nickel are released into the pore–water by reduction of oxides, diffuse towards the oxic/suboxic fronts

30   above and below where they precipitate, effectively removing these metals from the suboxic zone and concentrating them at the oxic/suboxic redox boundaries. We show that not only diffusive fluxes in the top part of deep–sea sediments modify the geochemical composition over time, but also diffusive fluxes of dissolved constituents from the basement into the bottom

layers of the sediment. Hence, paleoceanographic interpretation of sedimentary layers should carefully consider such deep secondary modifications in order to prevent misinterpretation as primary signatures.

1 Introduction

The heat flux from the mantle through the lithosphere into the ocean is high where the ocean crust is young and sediment cover sparse such as at spreading zones, and the heat flux typically decreases with age as the crust cools (e.g., Williams and von Herzen, 1974; Sclater et al., 1980; Davis et al., 1999). Ventilation of the basaltic crust by seawater is an important aspect of this cooling and is predicted to occur in off−axis settings up to an age of 65 Ma (e.g., Stein and Stein, 1992; Fisher et al., 2003; Hutnak et al., 2006). Most of the ocean floor has cooled over long periods and conversely, most ventilation of the basaltic crust occurs at low temperatures (Hasterok et al., 2011; Coogan and Gillis, 2018). Water percolating through the crust changes the chemistry of the basement and vice versa (Fisher and Wheat, 2010; Orcutt et al., 2013). Moreover, sediments overlying the basement may be modified by substances diffusing from the crust upwards such as oxygen whereas sedimentary products may diffuse down and interact with the crust (Ziebis et al., 2012; Mewes et al., 2016; Kuhn et al., 2017). Due to the vastness of the ocean floor, this low temperature ventilation may still have a large impact on the global geochemical and biogeochemical cycles (e.g., Baker et al., 1991). This impact is however poorly constrained. This is to a large extent due to sediments accumulating on the basement, making it less accessible and due to poor sediment permeability, they progressively insulate the crust, both thermally and hydrodynamically (Anderson et al., 1979). As a result, water can enter or leave the basement only where sediment cover remains thin or absent such as at seamounts, ridges and faults. Finally, diffusion of dissolved species from the basement into the sediments and vice versa modifies the compositions of both fluid and sediment and adds an extra aspect to the geochemical and biogeochemical impact of basement ventilation (e.g., Wheat and Mottl, 2000; Fisher et al., 2003; Wheat and Fisher, 2008; Kuhn et al., 2017).

1.1 Sediment geochemistry.

The ocean floor is subject to a continuous rain of reduced material, notably organic matter (OM). Sedimentary life harvests the energy stored in this reduced material by exploiting and catalysing the redox reactions possible, giving priority to the energetically most favourable redox pair (e.g., Froelich et al., 1979; Berner, 1980). In oxic sediments, the dominant redox process is aerobic respiration. Oxygen entering the sediment by diffusion is consumed on its way down and if sufficient OM is available it becomes exhausted resulting in an oxic/suboxic interface at depth. In a steady state situation, this interface keeps pace with sedimentation and its depth relative to the sediment surface remains constant (e.g., de Lange et al., 1983; Kasten et al., 2003). From this interface downwards successively energetically less favourable redox reactions follow, provided sufficient electron donors remain (e.g., Canfield and Thamdrup, 2009; Kasten et al., 2003). However, due to successively reduced activation energies, oxidation of OM will be increasingly less complete (e.g., Tegelaar et al., 1989;

Arnarson and Keil, 2007; Zonneveld et al., 2010). Dissolved redox products with remaining oxidation potential may diffuse to a zone with energetically more favourable redox reaction conditions and become further oxidised at the corresponding

65 redox front (e.g., the oxic/suboxic interface). Oxidation of immobile components requiring a high activation energy slows down or even stops, leading to long−term preservation as is the case of the more refractory OM below the oxic/suboxic interface (e.g., Arndt et al., 2013; Zonneveld et al., 2010).

Less input of reactive OM or lower sedimentation rates shift the balance between oxygen diffusion into the sediment and its benthic consumption deeper into the sediment. The result is increased oxygen exposure time of the sediments and a deeper

70 oxic/suboxic interface, which can reach depths of up to several meters and more (Fischer et al., 2009; Rühlemann et al., 2011; Ziebis et al., 2012; Mewes et al., 2014; d`Hondt et al., 2015; Mewes et al., 2016; Volz et al., 2018). The higher degree of OM degradation results in a more refractory residue. Conversely, OM degradation rates decrease more rapidly and to a larger extent with distance into the sediment as compared to regions with higher productivity and/or sedimentation rates (Mogollón et al., 2016).

75 In sediment−filled basins of the western flank of the Mid−Atlantic ridge at "North Pond" and in the deep−sea sediments of the Clarion Clipperton Zone (CCZ) oxygen was shown to not only diffuse down across the sediment−water interface but also upward into the basal sediments from the underlying oceanic basement (Ziebis et al., 2012; Mewes et al., 2016; Kuhn et al., 2017). For this upward diffusion both oxygen concentration profiles and redox dynamics involved differ from those near the sediment surface. Oxygen concentrations of the fluids circulating in the permeable crust were demonstrated to be lower than

80 those in the bottom water overlying the sediment surface due to partial consumption as a consequence of oxidation of reduced mineral phase contained in the crustal basalt (Fisher and Wheat, 2010; Orcutt et al., 2013; Mewes et al., 2016) The oxygen entering the sediment from below also encounters old, refractory OM and meets electron donors diffusing down from the redox−zones above. In this zone of upward diffusing oxygen, oxygen exposure time of OM increases downward and may be very long, up to equaling the age of the sediment involved in case this upward diffusive supply of oxygen never

85 ceased.

As yet the upward diffusion of oxygen from the basement has only been documented for a few abyssal ocean environments and its impact on the sediment composition, OM preservation/burial and biogeochemical cycles is largely under−explored and poorly understood (Kuhn et al., 2017; Mewes et al., 2016; Ziebis et al., 2012). This is to a large extent a result of coring practice and/or list of parameters typically measured onboard ship. Mostly, coring devices such as piston and gravity corers

90 are too short, or the sediment cover involved too thick to reach beyond the redox zones in the upper meters sediments and reach the deep oxic redox zone induced by the upward diffusion of oxygen from seawater circulating within the basement. Furthermore, although there is a long history of deeper drilling into the ocean sediments, and through them into the ocean crust (such as in the DSDP, ODP and IODP frameworks), the instances during which ex situ oxygen measurements were performed on these long sediment cores are extremely rare (e.g. Fischer et al., 2009; Ziebis et al., 2012; d'Hondt et al., 2013)

95 To overcome this problem, we went to the NE Pacific to the region of the CCZ in the framework of RV *Sonne* expedition SO240 (Kuhn et al., 2015) and among other pore−water and solid−phase components performed ex situ oxygen measurements on whole−round gravity cores (Fig. 1). Sedimentation rates in the CCZ are low ranging between 0.2 and 1.2 cm/ka (Mewes et al., 2014; Volz et al., 2018) thus combining a relatively thin sediment cover with a long period of sedimentation and oxygen penetration from below. As such, the lower oxidation front had ample time to move up and to get

100 into the reach of our coring devices. Sediments with such low sedimentation rates represent about 70% of the ocean floor (Bowles et al., 2014; Mewes et al., 2016) and conversely we hypothesise that extensive and long oxidation must be a widespread phenomenon in abyssal ocean deposits. Therefore, understanding the processes associated with upward oxygen supply from the basement into overlying sediments may be crucial for our understanding of global biogeochemical cycles and for properly interpreting marine sedimentary records/archive. To shed more light on the exchange between the basaltic

105 basement and the ocean as well as the role of the oceanic sediments herein, the oceanic basement and overlying sediments of the abyssal plain in the CCZ have been investigated seismically, thermally and geochemically during and after RV *Sonne* cruise SO240 in the framework of the project FLUM (FLUM project Kuhn et al., 2015; Fig1).

1.2 Study area

The oceanic basement underlying the sediments between the Clarion and the Clipperton Fracture Zones has been formed

110 from the late Cretaceous to the Miocene (Eittreim et al., 1992). The region hosts many seamounts and faults, which due to their steep topography are often barren of sediment on their slopes (e.g., Rühlemann et al., 2011). This allows seawater to circulate through the oceanic crust to enter or leave (Fisher and Wheat, 2010; Kuhn et al., 2017; Mewes et al., 2016). Sediment accretion is slow (typically a few mm/ka) due to the great distance from land, relatively great water depth, a low carbon flux to the sea floor of 1.5−1.8 mg C_{org} $m^{-2}d^{-1}$ (Lutz et al., 2007) and a sea floor below the carbonate compensation

115 depth. Meter−scale oxygen penetration into the sediment results in extensive organic matter mineralisation (TOC typically < 0.2%, and mostly below 0.4% at the surface) due to oxygen exposure times in the order of hundreds of thousands of years. (e.g., Müller and Mangini, 1980; Mewes et al., 2016; Volz et al., 2018).

In this paper we concentrate on the impact dissolved substances migrating from the crust have on the overlying sediment and vice versa sediment interactions to better understand the impact of seawater ventilation of oceanic crusts on global

120 biogeochemical cycles. We build upon recent insights on the low−temperature exchange of dissolved components between the basement and the overlying sediment and role of the sedimentary record (Mewes et al., 2016; Mogollón et al., 2016; Mewes et al., 2014; Fisher and Wheat, 2010; Kuhn et al., 2017; Volz et al., 2018). We pay special attention to the upward diffusion of oxygen from the basement to obtain a better insight on its impact on sediment composition, preservation/burial of OM and its relevance for global biogeochemical cycles.

2 Material and Methods

The oceanic crust in the region of investigation between 11.5°N, 116.3°W and 13.1°N, 119.6°W (Fig.1) is of middle to late Eocene age (17−21 Ma) (Barckhausen et al., 2013). Sediment cover is between 0 and 90 meters thick (Kuhn et al., 2015; Table 1). Sediments have been recovered during RV *Sonne* cruise SO240 (Kuhn et al., 2015) by means of box−, multiple−, gravity− and piston corer (Table 1; Fig 1). Cores consist generally of stiff and compact brown clays with depending on the MnO_2 contents lighter brown (less MnO_2) and darker (more MnO_2) sections (Kuhn et al., 2015). Of these, cores 22KL, 42SL, 72SL, 81SL and 96SL were taken close by or above a fault, cores 5SL, 35SL, 51SL, 53SL and 117SL were taken close to a seamount, core 69SL was taken near both a fault and a seamount and cores 9KL, 58SL, 65SL and 108SL were taken near neither a fault nor a seamount.

2.1 Oxygen analyses

Pore−water oxygen in the retrieved sediments was determined ex situ onboard using amperometric Clark−type oxygen sensors according to the procedure described by Ziebis et al. (2012), Mewes et al. (2014, 2016) and Volz et al. (2018). For conversion of the measured mV to mmol/l we used Eq. (1):

$$O_2 \text{ (mmol/l)} = V_d \text{ x } (V_{sat} - V_{Ar}) \text{ x } O_{2(sol)} \tag{1}$$

where V = sensor voltage at depth (V_d), under O_2 saturation (V_{sat}) and in argon (V_{ar}). $O_{2(sol)}$ is the oxygen solubility at the given temperature (measured), salinity (measured) and pressure conditions (atmospheric pressure) was calculated using the equation of García and Gordon (1992). Measurements were performed in an acclimatised room kept at 4 to 6°C.

2.2 Pore−water sampling and analyses

Upon recovery of the sediment cores, pore water was sampled using rhizons according to the procedure described by Seeberg−Elverfeldt et al. (2005) with a typical average pore diameter of 0.1 µm (Mewes et al., 2014). For NO_3^- analyses a QuAAtro Continuous Segmented Flow Analyser was used (Seal Analytical). Pore−water Mn^{2+} Ni^{2+} and Co^{2+} were determined after sample acidification with distilled HNO_3 by inductively coupled plasma optical emission spectrometry (ICP−OES; IRIS Intrepid ICP−OES Spectrometer, Thermo Elemental) using the NIST2702 standard as reference and following the procedures described by (Mewes et al., 2014).

2.3 Sediment analyses

For solid−phase element analysis, 50 mg of freeze−dried and homogenised bulk sediment were digested with a mixture of HF (0.5 ml, 40%, suprapur), HNO_3 (3 ml, 65%) and HCl (1.5ml, 30%, suprapur) at 220°C using a Mars Express microwave system (CEM) as described by Nöthen and Kasten (2011). Major and trace elements have been quantified in the laboratories

155 of the Alfred Wegener Institute Helmholtz Center for Polar and Marine Research (AWI) in Bremerhaven and the Jacobs University Bremen using inductively coupled plasma mass spectrometry (ICP−MS) and inductively coupled plasma optical emission spectrometry (ICP−OES), and at the Federal Institute for Geosciences and Natural Resources (BGR) in Hanover by quantitative XRF (X−ray Fluorescence Spectroscopy) (Rietveld, 1967). Cross calibration, achieved by quantifying the same elements with ICP−MS, ICP−OES and XRF for a few cores showed that the XRF measurements reliably reproduce the

160 changes in the elemental composition of the sediment.

The total carbon content (TC), the content of organic carbon (C_{org}) and the total sulphur (TS) content were determined using LECO CS 230 Carbon−Sulfur−Analyzer at the BGR. The samples were burned in a high−frequency−oven at 1800°−2200°C and the carbon and sulphur contents were determined using infrared−detection. Untreated samples were used to determine TC and TS. Another sample aliquot was treated with 2N HCl at 80°C to remove carbonate−carbon and subsequently

165 measured for C_{org} The difference between TC and C_{org} equals to carbonate−carbon.

Porosity has been calculated from the water content of samples with a known volume, corrected for salinity and using a bulk mineral density of 2.53 g cm^{-3} measured on core 22KL.

3 Results

The oxygen profiles of the cores analysed which are oxic throughout are highly asymmetric. From core top to bottom,

170 oxygen shows a strong decrease in the upper 30 centimetres and below a less pronounced decrease with depth leading to an interval of minimum oxygen concentrations between 2−3 m (Fig. 2). From there in most of these cores, a linear re−increase in oxygen concentrations is observed towards the bottom of the cores (51, 53SL, 117SL, 35SL, 81SL, 69SL, 96SL, Fig. 2). Core 5SL does not entirely follow these general patterns but shows an S−shaped oxygen profile (Fig. 2) we explain by assuming non−equilibrium from recent mass transport adding sediment at the location of this core, and/or by lateral transport

175 of oxygen and for that reason we do not take this core into further consideration.

At two sites, these upper and lower oxic zones are separated by an intermediate suboxic interval as indicated by the presence of Mn^{2+} in the pore−water (Fig. 3, 22KL, 42SL). There are five cores where the suboxic zone continues to the core bottom (9KL, 58SL, 65SL, 72SL 108SL). Of these seven cores that are partly suboxic, none has been retrieved close to a seamount, and none except for 22KL and 42SL has been retrieved from above a fault. Except for 58SL, all cores which are partly

180 suboxic show convex pore−water Mn^{2+} profiles whereby the profile from the upper oxic/suboxic interface downward is

steeper than the upward profile from the lower (extrapolated) oxic/suboxic interface. For core 22KL pore−water oxygen concentrations decrease linearly with depth. For site 58SL a downward decrease in Mn^{2+} concentration is absent and concentrations increase to the core bottom.

In all but two cores pore−water NO_3^- concentrations decrease downward from the core top (Figs 2, 3). For cores 22KL and 35SL the maximum is not at the sediment surface but, slightly below in the top meter and from this maximum the downward decrease commences (Figs 2, 3). In the cores with a suboxic zone the downward decrease in NO_3^- has a concave shape in the upper part, which is followed in the suboxic zone by a less steep linear decrease (9KL, 42SL, 58SL) or linear increase (22KL). The entirely oxic cores (35SL, 53SL, 117SL, 96SL) all display a linear downward decrease in NO_3^-. Extrapolation of the NO_3^- concentrations to the sediment−basement interface (see Table 1 for sediment thicknesses) provides values between 43 and 48 µmol/l at the interface for all oxic cores and for cores 22KL and 108SL. Core 5SL, and the remaining cores with a suboxic interval (lower extrapolated NO_3^- concentrations) do not follow this general pattern.

Pore−water trace metals that co−vary in their concentrations with Mn are Co and to a lesser extent Ni (Fig. 4). In combination with the solid−phase data of these elements, we see from top to bottom (if present, Fig. 4) an oxic zone (with for 22KL clearly decreasing TOC values), without free pore−water Mn and Co and with low pore−water Ni and elevated solid−phase Mn, Co, and Ni values, often with considerable scatter. Below this, a 'transition zone' (Fig. 4) is present with low oxygen, (and for core 22KL TOC low and constant) and solid−phase Mn, Co, Ni at the same level as in the oxic zone directly above whereas in the pore−water these elements mostly steeply decrease downward. Below this 'transition zone', solid−phase trace metal values are low and pore−water values are high. Below this, there is a sharp transition to oxic conditions without a transition zone. Like in the upper oxic zone, pore−water Mn and Co are below detection limit and dissolved Ni is low again, while the solid−phase values of all three elements increase (Fig. 4). Dissolved Fe has not been detected in any of the pore−waters, neither in the oxic nor in the anoxic sections. Solid−phase manganese for core 22KL shows an interval with low values in the suboxic interval.

4 Discussion

For most oceanic sediments oxygen is high at the sediment−water interface and steeply decreases to zero at depth (e.g., Wenzhöfer and Gludd, 2002) due to mineralisation of organic matter (OM). The oxygen profile is concave since oxygen is consumed over its entire oxic length (e.g., Froelich et al., 1979; Cai, and Sayles, 1996; Wenzhöfer and Gludd, 2002). The cores analysed in this study show the typical features of abyssal, carbon−starved oceans with sufficient deep−water ventilation. OM oxygen exposure times are long, OM degradation extensive, the remaining OM refractory and conversely sedimentary oxygen consumption rates low. As expected, we observe oxygen penetrating several meters into the sediments

210 (see also e.g. Fischer et al., 2009). Despite this, for some cores, sufficient degradable OM remains available to exhaust oxygen at depth. Below the oxic zone and with increasing sediment depth, we observe zones of denitrification and manganese reduction. (Froelich et al., 1979; Berner, 1980; Mogollón et al., 2016). However, iron reduction and sulphate reduction have not been observed due to the low content and reactivity of buried OM.

4.1 Pore−water oxygen

215 The presence of a second, upward directed diffusive flux of oxygen in many of the sediments investigated in our study and in some others suggests that oxygen is supplied from low−temperature seawater ventilation of the underlying basement. This seems to be a widespread phenomenon (Wheat and Fisher, 2008; Fisher and Wheat, 2010; Ziebis et al., 2012; Orcutt et al., 2013; Mewes et al., 2016; Kuhn et al., 2017). The interaction between the upward and downward directed oxygen profiles through time shapes the pore−water and solid−phase element profiles in the investigated sediments. Two types of

220 geochemical settings have been encountered in the investigated sediments. One type is represented by entirely oxic sediments with concave oxygen profiles (Fig. 2) and the other by cores with a suboxic zone of which some show below this a second oxic zone where oxygen concentrations increase towards the core bottom (Fig. 3). A compilation of the extension of the upward and downward pore−water oxygen and manganese profiles (Fig. 5) shows that the oxygen pore−water profiles from the core top downward are restricted to the upper three meters. The relatively constant thickness of the upper oxygen

225 pore−water profile (mostly 2−3 m), for the oxic cores suggests that the combination of OM flux to the sediment and benthic mineralisation, oxygen diffusion and sedimentation rate is relatively constant so that the system would turn into suboxic conditions somewhere below the upper 2−3 m. Although sedimentation rates in the area vary (Müller and Mangini, 1980; Mewes et al., 2016; Mewes et al., 2014; Volz et al., 2018), they are significantly lower than the rate at which oxygen diffuses into the sediments and thus have no significant influence on the oxygen penetration depth. This would imply that the

230 thickness of the sediment cover and the diffusive oxygen delivery from the basement into the overlying sediments, i.e., the steepness of the upward oxygen profile in the end determines if, and to what extent, a suboxic zone is present in the sediment.

In case oxygen consumption exceeds supply from above and below, two oxic/suboxic fronts are formed with the intermediate suboxic zone having free Mn^{2+} in pore−water. In a steady state situation, both fronts are metastable equilibria

235 between diffusion of reduced compounds produced in the suboxic zone to the oxidation front and consumption and diffusion of oxygen in the oxic zones. Whereas in the upper oxic zone the concave oxygen profile indicates that oxygen is consumed over the entire oxic zone due to the presence of more reactive OM close to the sediment surface, in the lower oxic zone the linear oxygen profiles indicate that oxygen consumption along the profile is insignificant compared to that at the front (Fig. 3). In combination with sediment thickness, this linearity allows us to extrapolate the profiles to the basement and calculate

240 basement oxygen concentrations for cores 35, 69 and 96 (using the seismic−based estimates of sediment thicknesses; Table

1). The thus obtained values (SL35, 66µmol/l @ 18m; 69SL, 204µmol/l @ 70m; 96SL, 25 µmol/l @ 15m) are considerably different, an observation also made for North Pond at the Mid−Atlantic Ridge (Ziebis et al., 2012; Orcutt et al., 2013). The differences may be caused e.g. by differences in fluid velocities, fluid path−length in the basement in combination with consumption of oxygen by reduced compounds in the basement or proximity to subsurface faults (Kuhn et al., 2017).

245 The influence of the sediment thickness on pore−water oxygen profiles is evident from the cores from areas with a thin sediment cover, 96SL, 5SL, 51SL, 53SL 117SL which are all entirely oxic (Table 1; Fig. 5) whereas longer cores appear oxic or partly suboxic. Cores 9KL, 65SL, 58SL and 108SL are the only cores from areas characterised by sediment thicknesses of > 15 m, that are neither close to a seamount nor above a fault, and they all have an intermediate suboxic interval. Oxic core 81SL and partly suboxic core 108SL have similar lengths, and have been taken close to each other (Fig.

250 1) whereby core 81SL has been taken above a fault in contrast to core 108SL. Considering the different lengths of the oxygen diffusion paths from below, we suggest that subsurface faults may facilitate upward oxygen diffusion, thus explaining the absence of a suboxic zone for core 81SL as already suggested by Kuhn et al. (2017). The presence of a fault may also explain why oxygen penetrates further upwards at site 72SL (near fault) compared to 65SL (no fault) despite both cores having been taken close together (Fig. 1) from sediments with similar thickness (72 and 71 m respectively; Fig 5). The

255 presence of an underlaying fault may also explain why 69SL is entirely oxic, despite the thickness of the sediment cover. Finally, it may explain why in core 22SL the lower oxic/suboxic interface is located at a shallower sediment depth than in core 9SL, despite the thicker sediment cover for core 22KL. Considering the differences between core 72SL (partly suboxic) and core 69SL (entirely oxic) which are both taken above a fault we need to take into account that the degree of facilitated diffusion by subsurface faults may differ so that sediments may differ in the degree to which they are suboxic. Especially in

260 combination with extension, pore volumes may increase, so that it is conceivable that faults increase sediment permeability. For these cores (> 10 m thickness), fluid advection may be neglected due to the low permeability of these sediments (Spinelli et al., 2004; Kuhn et al., 2017).

Apart from sediment thickness and the effect of faults, the oxygen concentration at the sediment−basement interface is a third variable determining the oxygen profile into the overlying sediments. This third variable depends a.o. on the flow rate,

265 length of way of the fluids in the basement, the amount of reducible compounds in the basin, and basement temperature, whereby the latter two variables also depend on basement age (e.g., Coogan and Gillis 2018). Near sites where oxygen−rich seawater enters the basement, such as near larger seamounts, oxygen concentrations at the sediment−basement interface will be highest (e.g., Fischer et al., 2003; Wheat et al., 2004). Since within the basement oxygen is consumed, and oxygen diffuses from the basement into the sediment, further away from these sites of inflow, oxygen concentrations at the

270 sediment−basement interface will be lower. This decrease in oxygen concentration per unit distance from the site of entrance will be faster if flow rates through the basement are low. Over time, the reactivity of the basement decreases as does temperature, and both may lead to a reduction of oxygen loss per unit distance through the sediment, provided a

simultaneous reduction in fluid flow rates doesn't compensate this. The oxygen diffusion is not necessarily vertical only. For instance, 69SL is taken close to a ridge system with a steep slope and sediment cover bay be sufficiently thin (Fig. 1) to

275 allow fluid venting from the basement into the ocean. As such it is conceivable that lateral oxygen diffusion, perpendicular to this venting, contributes to the upward oxygen profile for 69SL resulting in sediment columns in proximity of these venting systems that may be entirely oxic, possibly overruling the effect of sediment thickness.

The only core which in its pore−water Mn^{2+} profile shows no downward decrease and as such no signs of influence from below has been taken from the thickest sediment cover encountered (82 m) and as such the sediment is 10 m thicker than for

280 the other sites with thick sediments (65SL, 69SL, 72SL). Moreover, there are no faults or seamounts nearby. So, of all cores this one has the best prerequisites for having a suboxic zone that extends deep into the sediment. We therefore suppose that also for this location upward oxygen diffusion modifies the sediment but we are not able to see this since the pore−water Mn^{2+} maximum and subsequent downward decrease are found below the depth of the retrieved sediments/bottom of the core.

4.2 Pore−water nitrate

285 Usually in oxic sediments, nitrification of ammonium and diffusive loss of nitrate to the bottom water results in a nitrate maximum in the subsurface (Hensen et al., 2006). We find this back in the multicores (not shown) where values increase from 36 μmol/l at the sediment surface to reach maxima between 40 and 60 μmol/l at 10 to 50 cm depth. The absence of such a subsurface nitrate maximum for all piston− and gravity−cores but 22KL and 35SL (Fig. 2) is explained by the loss of surface sediments as a result of the core recovery procedure. As OM mineralisation slows down with increasing

290 sediment depth so does nitrate production. Furthermore, nitrate is diffusively lost to the overlying ocean bottom water (e.g., Hensen and Zabel 2000, Hensen et al., 2006), and to the deeper sediment. The subsurface pore−water nitrate maximum in the upper oxic zone of the cores reflects the balance between these three processes. For the entirely oxic cores, deeper in the sediment the linearly downward decreasing nitrate concentrations (Fig. 2) suggest the profiles to be driven by diffusion only, whereby nitrate is delivered to the basement fluid. Whereas the MUC core−tops indicate nitrate maximum concentrations of

295 35−40 μmol/l for ocean bottom waters (e.g., Hensen et al., 2006), extrapolation of the deeper linear nitrate profiles to the basement−sediment interface (from seismics; Kuhn et al., 2015) results in higher concentrations (43−48 μmol/l) for the sediment−basement interface. These values differ at most only 5 μmol/l suggesting the basement fluid to have a relatively constant nitrate concentration. It also implies that the seismic−based estimates of sediment thicknesses must be relatively accurate. Since the bottom−water nitrate concentrations are lower than those in the basement fluids we infer that there is a

300 net flux of nitrate from the sediment to the basement. This stability of nitrate concentrations at the sediment−basement interface contrasts with the variability of inferred oxygen concentrations at this interface suggesting very different dynamics such as a much stronger influence of processes in the basement on oxygen concentrations.

The cores with a suboxic zone (Fig. 3) have a more complex nitrate chemistry. From the nitrate maximum in the upper oxic zone well into the suboxic zone, the curvature of the profile becomes increasingly less (as also observed in some cores by

305   e.g. Mewes et al., 2014; Mogollón et al., 2016 for this region), indicating a decreasing contribution of aerobic nitrification and suboxic heterotrophic nitrification with depth. Extrapolation of the nitrate profile of core 108SL down to the anticipated depth of the basement−sediment interface provides values estimated between 42 and 47 μmol/l, which agrees with the values inferred from the entirely oxic cores. As such, the sediments represented by core 108SL are a source of nitrate for the basement fluid. For core 22KL, nitrate values reach below those inferred for the basement fluid. Here, the change from a

310   gentle decrease to a linear increase at 9 m core depth in core 22KL marks the point where upward nitrate diffusion from the basement equals downward diffusion and nitrate consumption. Linear extrapolation of this downward increase provides for the basement−sediment interface 44 μmol/l, which again agrees well with the values estimated from the entirely oxic cores/sites. However, in contrast to the oxic cores and core 108SL, the sediments represented by 22SL are a sink for basement−fluid nitrate. For the remaining cores with a suboxic zone (9KL, 42SL, 58SL, 65SL, and 72SL), denitrification is

315   even more substantial and minimum nitrate values always reach below those inferred for the basement fluid. We infer for the sediments below these cores a nitrate profile analogous to that seen in 22KL. However, whereas the nitrate minimum occurs within 22KL, we infer that these other cores did not reach sufficiently deep reach the nitrate minimum. From this minimum, (anticipated to be located below the maximum core depth), we infer a linear downward nitrate increase towards the basement — suggesting that the basement fluid represents a nitrate source.

320   There appears to be a clear linear relationship between the minimum pore−water nitrate concentration measured and the maximum pore−water manganese concentration (Fig. 6), which roughly suggests that for each μmol/l increase in manganese, nitrate decreases by also one μmol/l and this suggests a coupling between the manganese and nitrate cycles. The ratio is very different from the manganese mediated denitrification where 2.5 manganese are needed to consume one nitrate to produce 0.5 nitrogen molecule (e.g., Mogollón et al., 2016). We note that such an opposite relation can be induced by two processes:

325   (1) Oxidation by O_2 increases NO_3^- (from NH_4^+) and decreases Mn^{2+} (producing MnO_2) whereas (2) OM degradation consumes NO_3^- (producing NH_4^+) and produces Mn^{2+} (from MnO_2) (see e.g., Mogollón et al., 2016). Apparently, the long−term dynamic equilibria between these processes result in the observed net relation between the minimum pore−water nitrate concentration measured and the maximum pore−water manganese concentration in the sediments of this region.

Thus, we observe that some sediments deliver nitrate to the basement whereas others take up nitrate from the basement. We

330   also observe that the inferred nitrate values in the basement are higher than those in the ocean bottom waters, which implies that after entering the basement, the basement fluids get enriched in nitrate. We infer, therefore, that overall, the nitrate uptake from the basement by the sediment is less than the nitrate delivery to the basement by the sediment so that the basement gets enriched in nitrate relative to the ocean bottom waters. This nitrate enrichment can also be observed for the Cocos Ridge (Wheat and Fisher, 2008).

4.3 Pore–water manganese and iron

While in sediments with sufficient reactive OM the manganese reduction zone is followed by iron reduction, there is no evidence of this latter process in the cores investigated — i.e. the abundance of electron donors in the form of OM is too low to induce Fe reduction. In all cases where dissolved manganese is present in the pore–water, we observe a maximum followed by a decrease with depth (Fig. 3). However, in those cases where we can follow this decrease further to zero, it is followed by oxygenated sediments and not by free iron. Consequently, we infer that in the complete region of this study insufficient reductive power is available to induce iron reduction.

4.4 Nickel and cobalt in pore water and solid phase

Both pore–water and solid–phase nickel and cobalt in the suboxic cores tend to behave similar as/to manganese (Fig. 4), which agrees with the assumption that both metals are preferentially associated with the Mn oxide phase in the sediment (Aplin and Cronan, 1985; Koschinsky et al., 2001). In the suboxic zone, Mn oxide reduction also releases dissolved Ni^{2+} and Co^{2+} into the pore–water. Especially cobalt behaves similar to manganese, both clearly showing the 'transition zone' between the upper oxic zone and the suboxic zone (upper front). We call this a 'transition zone' since these elements are still present in the pore–water but already show elevated solid–phase contents. Nickel is much less bound to the oxidation fronts and seems to remain more mobile in the pore waters at higher oxygen levels than is the case for manganese and cobalt. The reason for this may be oxidation of pore–water Co^{2+} to Co^{3+} when bound to the Mn oxide phase in the sediment, which is a much more efficient scavenging process compared to simple adsorption, such as for Ni^{2+} (Murray and Dillard, 1979). Experiments with manganese oxide rich sediments also showed that the bonding of Ni is on average weaker and more easily reversible than for Co, and oxidation of Co during sorption on Mn oxides was confirmed (Kay et al., 2001).

4.5 Stability of the upper and lower redox fronts

The absence of a 'transition zone' for cobalt and manganese between the suboxic zone and the lower oxic zone (lower front) illustrates that the upper front is much more dynamic than the lower front. The lower front is the result of a very long route of oxygen transport from the ocean into and through the basement. As such, changes in ocean water oxygen arrive at the lower front delayed and with lower amplitude and as a consequence of oxidation of reduced mineral phases in the crust also with lower concentrations. As a result, the lower front is much more stable and probably foremost moves slowly but steadily upward, oxidising the OM residue left behind when the upper front moved upwards with ongoing sedimentation. The oxygen from the upper front has a much shorter route from its oceanic source and is thus much more subject to changes in deep–water oxygen content and/or marine production.

4.6 Different aspects of the top and bottom redox zonations

Considering the above, we may add geochemical details to the conceptual model of low−temperature circulation/diffusion of
seawater/fluids and their components through ocean crust and overlying sediments that was presented by Fisher and Wheat
(2010) (Fig. 7). The classical model of a succession of redox zones from the ocean floor into the sediment has to be extended
by adding a similar reversed zonation scheme from the basement−sediment interface into the sediment for those regions
where basement fluids are oxic. However, there are some marked differences between the redox succession from the
sediment surface downwards, and that from the basement and lower/overlying sediments upwards.

At the sediment surface the OM is fresh, highly reactive and subject to aerobic degradation first (Mewes et al., 2014;
Mogollón et al., 2016). With ongoing sedimentation and concurrent upward movement of the oxic zone, progressively less
energetically favourable redox processes follow. Here, the reaction time is often too short for a given redox process to
consume all available substrate. Reduced species that can't be oxidised by the next, energetically less favourable redox pair
will remain, resulting in a surplus of reduced material that becomes fossilised at depth.

In contrast to this, oxygen penetrating from the basement into the sediment encounters the oldest sediment first. Compared to
the sediment surface, reaction time is long and may equal sediment age. Here, not oxygen exposure time is limiting the
degree to which the substrate (OM) can be oxidised but the reactivity of the substrate. From the basement, the successively
energetically less favourable redox zones follow each other upward so that at a particular depth, with time, progressively
stronger oxidants may be expected, each consuming the fossilised reduced species (such as OM) that were left by the
upwards migrating redox zones near the sediment surface. It should be noted that the fossilisation process may have changed
the reactivity and degradability of the fossilised species over time (e.g., in sediments where sulphate reduction occurs (not in
our sediments), natural sulphurisation may have cross−linked residual organic matter reducing its degradability by
microorganisms (Zonneveld et al., 2010)). The order of redox processes upwards thus mirrors that from the sediment−water
interface downwards. Considering the large amount of time available, consumption in the lower oxic zone (from the
basement upwards) should be negligible so that the oxygen profile will approach linearity up to the oxic/anoxic interface
above. In sediments that are carbon−starved and have virtually no oxidisable organic material left in the solid phase. Thus,
the front position is primarily a balance between the downward migration/burial of oxidisable species and upward oxygen
flux from the basement. This is what we observe at site 22KL. Here, the downward directed profile of Mn, Co, Ni and other
reduced species become linear already in the suboxic zone and meet a counter−directed linear upward oxygen diffusion
profile. If oxygen supply from below increases, the oxygen flux from below may meet the upper oxic zone. Thus, in the
CCZ, the entirely oxic cores display a configuration where the balance between supply of reduced species to the sediment,
oxygen supply and sedimentation rate is such that a suboxic zone is absent as is a pool of reduced fossilised material. Here,
the upward oxygen flux meets the downward flux at the point of equal flux. The lower profile contributes here to the aerobic
degradation at the sediment−water interface.

395 If in such entirely oxic sediments the upward oxygen flux becomes less, the oxygen minimum and the downward directed oxygen diffusion will extend downward where it will meet increasingly refractory carbon since oxygen exposure time by the lower oxygen profile increases towards the basement. Where the residual carbon is very refractory, this downward profile will become quasilinear. Despite very low oxygen consumption in such sediments, if they are sufficiently thick, the system may become suboxic eventually. Since this suboxic zone is formed where previously the oxygen from below had

400 exhaustively removed electron donors. Manganese re−mobilisation may be very slow relative to diffusion, or even absent due to lack of electron donors and thus, we expect to encounter a suboxic sediment where porewater manganese is undetectable, a situation that may apply to core 81SL (Fig. 2).

5 Conclusions

Analyses of the concentrations of oxygen, nitrate, manganese, nickel and cobalt in pore waters and the solid−phase of

405 sediments from the CCZ have been summarised in a conceptual graph (Fig. 8) and show:

1. An upper oxygen profile due to oxygen penetrating the sediments from the ocean bottom water downwards and a lower oxygen profile due to oxygen penetrating from the basement upwards.

2. The length of the upper profile (2−3 m) to be relatively constant, the length of the lower profile to be very variable; the latter as a result of facilitated penetration near faults, differences in basement conditions such as fluid flow rate, path length

410 and basement oxygen consumption.

3. Where the upper and lower oxygen profiles meet, sediments are entirely oxic and organic carbon mineralisation is exhaustive. Nitrate production is larger than denitrification so that the sediments are a source of nitrate for the ocean bottom water and basement fluid.

4. Where the upper and lower oxygen profiles do not meet, they are separated by an intermediate suboxic zone with free

415 pore−water manganese and cobalt. Here denitrification continues and may be in excess of nitrate production so that the basement fluid delivers nitrate to the sediment.

5. Extrapolation of nitrate profiles indicates that the nitrate concentrations at the basement−sediment interface are relatively constant (43−48 μmol/l) and higher than in the ocean bottom waters and we conclude that overall more nitrate goes from the sediment to the basement (see conclusion 3) than *vice versa* (see conclusion 4).

420 6. The behaviour of the upper and lower oxic/suboxic transitions is very different. The upper oxic/anoxic redox boundary is at the end of a curved oxygen profile. The redox boundary moves up with sedimentation, leaving unoxidised OM behind in the manganese reduction zone below. Moreover, due to the relatively short distance between bottom water and the front, the position of the upper front is sensitive to changes in bottom water oxygen content and as such relatively unstable. The lower oxic/anoxic redox boundary is at the end of a linear oxygen profile, and it moves up as a result of lacking (sufficiently labile)

425 oxidisable material further down. It leaves behind an 'energetic desert' without further oxidation potential. The long transport route of bottom water oxygen, via basement fluid (advection) into the sediment and to the lower oxic/suboxic transition (diffusion), strongly buffers amplitude and frequency of changes in oxygen content, so that the lower transition is much more stable than the upper front.

7. Over time, manganese, nickel and cobalt diffuse from the suboxic zone to the upper and lower redox fronts/transitions
430 where they are oxidised and precipitate. At the upper transition they add to the manganese, cobalt and nickel that were deposited by sedimentation. With this transition moving upward with sedimentation, these elements re–enter the suboxic zone, remobilise and move up to the oxic/suboxic transition again, leading to a continuous increasing in solid–phase contents of these elements near the redox front. With the lower transition moving upwards, these elements remain fixed in the oxidised sediment below, resulting in a permanent loss of these elements from the suboxic zone.

435 8. Since in the region between the Clarion and Clipperton Fracture Zones sediment cover is generally thin and sedimentation rates are generally low, we are mostly able to observe the upper oxygen profile and accompanying redox zone as well as in reverse the lower redox zone and oxygen profile, each with its associated set of phenomena such as nitrate diffusion into the basement fluid. In many other ocean regions sediments are thicker and productivity higher so that the lower oxygen profile will be below the reach of the gravity– or piston–coring device due to a more complete redox zonation reaching deeper into
440 the sediment and drilling is needed to reach the successive redox zones as well as the reversed redox zonation followed by the deep oxygen profile to the basement (provided sufficient oxygen is provided by the basement). We are just beginning to understand the impact of this deep redox zonation on the biogeochemical cycles of carbon and nitrogen as well as the distribution of carbon and other elements (such as manganese and associated metals such as nickel and cobalt and, in organically richer sediments, iron and sulphur) in the deep sediments. Fortunately, deep drilling (e.g., through international
445 consortia like DSDP, ODP and IODP) logistically and financially enable access to these deeper sediments to investigate to what extent theories and hypotheses erected on the basis of shallower settings are applicable for the majority of the ocean floor. Considering the potential area involved this warrants a substantial research effort.

9. Our study has pointed out that not only diffusive fluxes in the top part of deep–sea sediments modify the geochemical composition over time, but also diffusive fluxes from the basement into the bottom layers of the sediment. Hence,
450 paleoceanographic interpretation of sedimentary layers should carefully consider such secondary modifications in order to prevent misinterpretation as primary signatures.

6 Code and Data Availability

Data are available at https://doi.pangaea.de/10.1594/PANGAEA.xxxxxx. A doi has been applied but has not yet been issued.

7 Author Contributions

455   Gerard J. M. Versteegh interpreted the data and wrote the manuscript. Inken Preuss carried out the porewater analyses, Thomas Kuhn performed the solid phase analyses. Sabine Kasten and Andrea Koschinsky, together with Thomas Kuhn, designed and supervised the project. All authors discussed data and contributed to the manuscript at different stages.

8 Competing Interests

The authors declare they have no competing interests.

460   **9 Acknowledgments**

We thank captain Lutz Mallon and his crew for the excellent co−operation and the pleasant atmosphere during RV *Sonne* cruise SO240. We also appreciate the enthusiasm and engagement of the scientific participants of the expedition. This work was funded by the German Federal Ministry for Education and Science (BMBF) under grant no. 03G0240A−C and by internal funding of the Federal Institute for Geosciences and Natural Resources (BGR) under the project no. A−0203002.A.

465   We acknowledge further financial support from the Helmholtz Association (Alfred Wegener Institute Helmholtz Centre for Polar and Marine Research).

References

Anderson, R. N., Hobart, M. A., Langseth, M. G.: Geothermal convection through oceanic crust and sediments in the Indian Ocean, Science, 204, 828−832, 1979, doi: 10.1126/science.204.4395.828.

470   Aplin, A. C., Cronan, D. S.: Ferromanganese oxide deposits from the Central Pacific Ocean, II. Nodules and associated sediments, Geochim. Cosmochim. Acta, 49, 437−451, 1985, doi: 10.1016/0016-7037(85)90035-3.

Arnarson, T. S., Keil, R. G.: Changes in organic matter−mineral interactions for marine sediments with varying oxygen exposure times, Geochim. Cosmochim. Acta, 71, 3545−3556, 2007, doi: 10.1016/j.gca.2007.04.027.

Arndt, S., Jørgensen, B. B., LaRowe, D. E., Middelburg, J. J., Pancost, R. D., Regnier, R.: Quantifying the degradation of
475   organic matter in marine sediments: A review and synthesis, Earth−Sci. Rev., 123, 53−86, 2013, doi: 10.1016/j.earscirev.2013.02.008.

Baker, P. A., Stout, P. M., Kastner, M., Elderfield, H.: Large−scale lateral advection of seawater through oceanic crust in the central equatorial Pacific, Earth Planet. Sci. Lett., 105, 522−533, 1991, doi: 10.1016/0012-821X(91)90189-O.

Barckhausen, U., Bagge, M., Wilson, D. S.: Seafloor spreading anomalies and crustal ages of the Clarion−Clipperton Zone,
480 Mar. Geophys. Res., 34, 79−88, 2013, doi: 10.1007/s11001-013-9184-6.

Berner, R. A.: Early Diagenesis. A Theoretical Approach. Princeton University Press, Princeton NJ, 1980.

Bowles, M. W., Mogollón, J. M., Kasten, S., Zabel, M., Hinrichs, K. −U.: Global rates of marine sulfate reduction and
implications for sub–sea−floor metabolic activities, Science, 344, 889−891, 2014, doi: 10.1126/science.1249213.

Cai, W. −J., Sayles, F. L.: Oxygen penetration depths and fluxes in marine sediments, Mar. Chem., 52, 123−131, 1996, doi:
485 10.1016/0304-4203(95)00081-X.

Canfield, D. E., Thamdrup, B.: Towards a consistent classification scheme for geochemical environments, or, why we wish
the term 'suboxic' would go away, Geobiol., 7, 385−392, 2009, doi: 10.1111/j.1472-4669.2009.00214.x.

Coogan, L. A. Gillis, K. M. Low−Temperature Alteration of the Seafloor: Impacts on Ocean Chemistry, Annu. Rev. Earth
Planet. Sci., 46. 21−45, 2018, doi: 10.1146/annurev- earth- 082517- 010027.

490 D'Hondt, S., Inagaki, F., Alvarez Zarikian, C., IODP Expedition 329 Scientific Party: IODP Expedition 329: Life and
Habitability Beneath the Seafloor of the South Pacific Gyre. Scientific Drilling 15, 4−10, 2013, doi:
10.2204/iodp.sd.15.01.2013.

D'Hondt, S., Inagaki, F., Zarikian, C. A., Abrams, L. J., Dubois, N., Engelhardt, T., Evans, H., Ferdelman, T., Gribsholt, B.,
Harris, R. N. ,Hoppie, B., Hyun, J. −H., Kallmeyer, J., Kim, J., Lynch, J. E., McKinley, C., Mitsunobu, S., Morono, Y.,
495 Murray, R. W., Pockalny, R., Sauvage, J., Shimono, T., Shiraishi, F., Smith, D., C. Smith−Duque, C., Spivack, A. J.,
Steinsbu, B. O., Suzuki, Y., Szpak, M., Toffin, L., Uramoto, G., Yamaguchi, Y. T., Zhang, G. −L., Zhang, X. −H., Ziebis,
W.: Presence of oxygen and aerobic communities from sea floor to basement in deep−sea sediments, Nature Geoscience 8,
299−304, 2015, doi: 10.1038/NGEO2387.

Davis, E. E., Chapman, D. S., Wang, K., Villinger, H., Fisher, A. T., Robinson, S. W., Grigel, J., Pribnow, D., Stein, J.,
500 Becker: Regional heat flow variations across the sedimented Juan de Fuca Ridge eastern flank: Constraints on lithospheric
cooling and lateral hydrothermal heat transport, J. Geophys. Res. − Atm., 104, 17675−17688, 1999, doi:
10.1029/1999JB900124.

Eittreim, S. L., Ragozin, N., Gnibidenko, H. S., Helsley, C. E.: Crustal age between the Clipperton and Clarion Fracture
Zones, Geophys. Res. Lett., 19, 2365−2368, 1992, doi:10.1029/92GL02928.

505 Fischer, J. P., Ferdelman, T. G., D'Hondt, S., Røy, H., Wenzhöfer, F.: Oxygen penetration deep into the sediment of the
South Pacific gyre, Biogeosci., 6, 1467−1478, 2009, doi: 10.5194/bg-6-1467-2009.

Fisher, A. T., Davis, E. E., Hutnak, M., Spiess, V., Zühlsdorff, L., Cherkaoui, A., Christiansen, L., Edwards, K., Macdonald, R., Villinger, H., Mottl, M. J., Wheat, C. G., Becker, K.: Hydrothermal recharge and discharge across 50 km guided by seamounts on a young ridge flank, Nature, 421, 618−621, 2003, doi: 10.1038/nature01352.

510 Fisher, A. T., Wheat, C. G.: Seamounts as conduits for massive fluid, heat, and solute fluxes on ridge flanks, Oceanogr., 23, 74−87, 2010, doi: 10.5670/oceanog.2010.63.

Froelich, P. N., Klinkhammer, G. P., Bender, M. L., Luedtke, N. A., Heath, G. R., Cullen, D., Dauphin, P., Hammond, D., Hartman, B., Maynard, V.: Early oxidation of organic matter in pelagic sediments of the eastern equatorial Atlantic: suboxic diagenesis, Geochim. Cosmochim. Acta, 43, 1075−1090, 1979, doi: 10.1016/0016-7037(79)90095-4.

515 García, H. E., Gordon, L. I.: Oxygen solubility in seawater: Better fitting equations, Limnol. Oceanogr., 37, 1307−1312, 1992, doi: 10.4319/lo.1992.37.6.1307.

Hasterok, D., Chapman, D. S., Davis, E. E.: Oceanic heat flow: Implications for global heat loss, Earth Planet. Sci. Lett., 311, 386−395, 2011, doi: 10.1016/j.epsl.2011.09.044.

Heller, C., Kuhn, T., Versteegh, G. J. M., Wegorzewski, A. V., Kasten, S.: The geochemical behavior of metals during early
520 diagenetic alteration of buried manganese nodules, Deep Sea Res. I, 142, 16−33, 2018, doi: 10.1016/j.dsr.2018.09.008.

Hensen, C., Zabel, M., Schulz, H. D.: A comparison of benthic nutrient fluxes from deep−sea sediments off Namibia and Argentinia. Deep−Sea Research II 47, 2029−2050, 2000, doi: 10.1016/S0967-0645(00)00015-1.

Hensen, C., Zabel, M., Schulz, H. N., Early Diagenesis at the Benthic Boundary Layer: Oxygen, Nitrogen, and Phosphorus in Marine Sediments . In: Schulz H. D., Zabel M. (eds.), Marine Geochemistry, Springer, Heidelberg, pp. 207−240, 2006,
525 doi: 10.1007/3-540-32144-6_6.

Hutnak, M., Fisher, A. T., Zühlsdorff, L., Spiess, V., Stauffer, P. H., Gable, C. W.: Hydrothermal recharge and discharge guided by basement outcrops on 0.7–3.6 Ma seafloor east of the Juan de Fuca Ridge: Observations and numerical models, Geochemistry, Geophysics, Geosystems, 7, 2006, doi: 10.1029/2006GC001242.

Kasten, S., Zabel, M., Heuer, V., Hensen, C.: Processes and signals of non−steady state diagenesis in deep−sea sediments,
530 in: Wefer G., Mulitza S., Rathmeyer V. (eds.), The South Atlantic in the Late Quaternary, Springer, Berlin, pp. 431−459, 2003, doi: 10.1007/978-3-642-18917-3_20.

Kay, J., Conklin, M. H., Fuller, Christopher C, O'Day, P. A.: Processes of nickel and cobalt uptake by a manganese oxide forming sediment in Pinal Creek, Globe Mining District, Arizona, Environmental Science and Techology, 35, 4719−4725, 2001, doi: 10.1021/es010514d.

535   Koschinsky, A., Fritsche, U., Winkler, A.: Sequential leaching of Peru Basin surface sediment for the assessment of aged and fresh heavy metal associations and mobility, Deep Sea Research II: 48, 3683−3699, 2001, doi: 10.1016/S0967-0645(01)00062-5.

Kuhn, T., Bösel, J., Dohrmann, I., Filsmair, C., Fronzek, J., Gerken, J., Goergens, R., Hartmann, J. F., Heesemann, B., Heller, C., Heyde, I., Janssen, A., Kasten, S., Kaul, N., Kevel, O., Kleint, C., Lückge, A., Müller, P., Preuss, I. −M.,
540   Purkiani, K., Ritter, S., Rühlemann, C., Schwab, A., Sing, R., Stegger, U., Sturm, S., Uhlenkott, K., Villinger, H., Vink, A., Wedemeyer, H., Wegorzewski, A.: SO240 − Flum: Low−temperature. Fluid. Circulation. at Seamounts and Hydrothermal Pits:. Heat Flow Regime, Impact on Biogeochemical Processes and its Potential Influence on the Occurrence and. Composition of Manganese Nodules in the Equatorial Eastern Pacific, 1−185, 2015, doi: 10.2312/cr_so240.

Kuhn, T., Versteegh, G. J. M., Villinger, H., Dohrmann, I., Heller, C., Koschinsky, A., Kaul, N., Ritter, S., Wegorzewski, A.
545   V., Kasten, S.: Widespread sea−water circulation in 18–22 Ma oceanic crust: Impact on heat flow and sediment geochemistry, Geology, 45, 799−802, 2017, doi:10.1130/G39091.1.

de Lange, G. J.: Geochemical evidence of a massive slide in the southern Norwegian Sea. Nature 305, 420−422, 1983, doi: 10.1038/305420a0.

Lutz, M. J., Caldeira, K., Dunbar, R. B., Behrenfeld, M. J.: Seasonal rhythms of net primary production and particulate
550   organic carbon flux describe the biological pump efficiency in the global ocean. J. Geophys. Res. Oceans, 112, C10011, 2007, doi: 10.1029/2006JC003706.

Mewes, K., Mogollón, J. M., Picard, A., Rühlemann, C., Kuhn, T., Nöthen, K., Kasten, S.: Impact of depositional and biogeochemical processes on small scale variations in nodule abundance in the Clarion-Clipperton Fracture Zone, Deep Sea Res. I: 91, 125−141, 2014, doi:10.1016/j.dsr.2014.06.001.

555   Mewes, K., Mogollón, J. M., Picard, A., Rühlemann, C., Eisenhauer, A., Kuhn, T., Ziebis, W., Kasten, S.: Diffusive transfer of oxygen from seamount basaltic crust into overlying sediments: An example from the Clarion–Clipperton Fracture Zone, Earth Planet. Sci. Lett., 433, 215−225, 2016, doi:10.1016/j.epsl.2015.10.028.

Mogollón, J. M., Mewes, K., Kasten, S.: Quantifying manganese and nitrogen cycle coupling in manganese−rich, organic carbon−starved marine sediments: Examples from the Clarion−Clipperton fracture zone, Geophys. Res. Lett., 43, 7114−
560   7123, 2016, doi:10.1002/2016gl069117.

Murray, J. W., Dillard, J. G.: The oxidation of cobalt(II) adsorbed on manganese dioxide, Geochim. Cosmochim. Acta, 43, 781−787, 1979, doi:10.1016/0016-7037(79)90261-8.

Müller, P. J., Mangini, A.: Organic carbon decomposition rates in sediments of the pacific manganese nodule belt dated by ^{230}Th and ^{231}Pa, Earth Planet. Sci. Lett., 51, 94−114, 1980, doi: 10.1016/0012-821X(80)90259-9.

565   Nöthen, K., Kasten, S.: Reconstructing changes in seep activity by means of pore water and solid phase Sr/Ca and Mg/Ca ratios in pockmark sediments of the Northern Congo Fan, Mar. Geol., 287, 1−13, 2011, doi: 10.1016/j.margeo.2011.06.008.

Orcutt, B. N., Wheat, C. G., Rouxel, O., Hulme, S., Edwards, K. J., Bach, W.: Oxygen consumption rates in subseafloor basaltic crust derived from a reaction transport model, Nat. Commun., 4, 2539, 2013, doi:10.1038/ncomms3539.

Rietveld, H. M.: Line profiles of neutron powder-diffraction peaks for structure refinement, Acta Crystallogr., 22, 151−152,
570   1967, doi: 10.1107/S0365110X67000234.

Rühlemann, C., Kuhn, T., Wiedicke, M., Kasten, S., Mewes, K. and Picard, A. (2011) Current status of manganese nodule exploration in the German license area. Proceedings of the Ninth (2911) ISOPE Ocean Mining Symposium, Maui, Hawaii, USA, June 19−24, 2011, 168−173.

Sclater, J. G., Jaupart, C., Galson, D.: The heat flow through oceanic and continental crust and the heat loss of the Earth,
575   Rev. Geophys. Rev. Geophys, 18, 269−311, 1980, doi: 10.1029/RG018i001p00269.

Seeberg−Elverfeldt, J., Schlüter, M., Feseker, T., Kölling, M.: Rhizon sampling of porewaters near the sediment−water interface of aquatic systems, LOM3. Limnol. Oceanogr.: Methods., 3, 361−371, 2005, doi: 10.4319/lom.2005.3.361.

Spinelli, G. A., Giambalvo, E. R., Fisher, A. T.: Sediment permeability, distribution, and influence on fluxes in oceanic basement. In: Davis E. E., Elderfield H. (eds.), Hydrogeology of the oceanic lithosphere, Cambridge University Press,
580   Cambridge151−188, 2004.

Stein, C. A., Stein, S.: A model for the global variation in oceanic depth and heat flow with lithospheric age, Nature, 359, 123−129, 1992, doi: 10.1038/359123a0.

Tegelaar, E. W., de Leeuw, J. W., Derenne, S., Largeau, C.: A reappraisal of kerogen formation, Geochim. Cosmochim. Acta, 53, 3103−3106, 1989, doi: 10.1016/0016-7037(89)90191-9.

585   Volz, J. B. , Mogollón, J. M. , Geibert, W. , Martínez Arbizu, P. , Koschinsky, A., Kasten, S.: Natural spatial variability of depositional conditions, biogeochemical processes and element fluxes in sediments of the eastern Clarion−Clipperton Zone, Pacific Ocean, Deep Sea Research Part I, 140, 159−172, 2018, doi: 10.1016/j.dsr.2018.08.006.

Wenzhöfer, F. and Gludd, R. N.: Benthic carbon mineralization in the Atlantic: a synthesis based on in situ data from the last decade. Deep Sea Research Part I: Oceanographic Research Papers 49, 1255−1279, 2002, doi: 10.1016/S0967-
590   0637(02)00025-0.

Wheat, C. G., Fisher, A. T.: Massive, low−temperature hydrothermal flow from a basaltic outcrop on 23 Ma seafloor of the Cocos Plate: Chemical constraints and implications, Geochemistry, Geophysics, Geosystems, 9, 1−16, 2008, doi: 10.1029/2008GC002136.

Wheat, C. G., Mottl, M. J.: Composition of pore and spring waters from Baby Bare: global implications of geochemical fluxes from a ridge flank hydrothermal system, Geochim. Cosmochim. Acta, 64, 629−642, 2000, doi: 10.1016/s0016-7037(99)00347-6.

Williams, D. L., von Herzen, R. P.: Heat Loss from the Earth: New Estimate, Geology, 2, 327−328, 1974, doi: 10.1130/0091-7613(1974)2<327:HLFTEN>2.0.CO;2.

Ziebis, W., McManus, J., Ferdelman, T., Schmidt−Schierhorn, F., Bach, W., Muratli, J., Edwards, K. J., Villinger, H.: Interstitial fluid chemistry of sediments underlying the North Atlantic gyre and the influence of subsurface fluid flow, Earth Planet. Sci. Lett., 323−324, 79−91, 2012, 10.1016/j.epsl.2012.01.018.

Zonneveld, K. A. F., Versteegh, G. J. M., Kasten, S., Eglinton, T. I., Emeis, K. C., Huguet, C., Koch, B. P., de Lange, G. J., de Leeuw, J. W., Middelburg, J. J., Mollenhauer, G., Prahl, F. G., Rethemeyer, J., Wakeham, S. G.: Selective preservation of organic matter in marine sediments − processes and impact on the fossil record, Biogeosci., 7, 483−511, 2010, doi:10.5194/bg-7-483-2010.

Table 1: Sediment cores analysed.

Working Area	Core	Latitude (N)	Longitude (W)	Water depth (m)	Length (cm)	Heat flow (Wm^{-2})	Sediment thickness (m)	Length upper oxic zone (m)	Lower ox. front (m)	Length lower oxic zone (m)
1	5SL	13° 10.525'	118° 06.705'	4287	756	-	<10	2	n.a.[1]	8?
1	9KL	13° 10.524'	118° 10.104'	4335	1187	5	17	0.5	14[2]	3
1	22KL	13° 10.527'	118°08.184'	4302	1301	10	24	1.5	10	14
1	51SL	13° 10.526'	118° 06.584'	4286	537	42	<10	3	n.a.	7
1	53SL	13° 10.508'	118° 06.110'	4273	482	54.8	8	2.5	n.a.	5
1	117SL	13° 11.103'	118° 05.992'	4271	600	195	-	2	n.a.	n.a.
2	35SL	12° 54.128'	118° 24.791'	4319	982	9	18	2.5	n.a.	15.5
2	42SL	12° 51.249'	118° 23.976'	4290	1066	37	29	<0.5	7	22
3	58KL	12° 53.216'	119° 08.351'	4309	1244	50	83	3?	?	?
3	65SL	12° 56.107'	119° 08.884'	4293	1275	65	71	3?	?	?
3	69SL	12° 39.855'	119° 13.374'	4275	1265	130	70	3	n.a.	67
3	72SL	12° 55.597'	119° 08.833'	4294	853	85	72	2	?	?
4	81SL	11° 50.064'	116° 32.890'	4355	1346	91	20	2(4?)	n.a.	17
4	96SL	11° 49.260'	117° 13.195'	4145	980	80	<15	3	n.a.	<12
4	108SL	11° 48.796'	116° 31.767'	4326	1038	60	20	3	16[2]	4

[1] n.a. = not available; [2] Extrapolated from porewater Mn profile.

Table 2: Linear regressions and extrapolated NO_3^- concentrations at the sediment base. Regressions are based on the lower, linear part of the O_2 and NO_3^- profiles. Whereby: Concentration in µmol / L = a * (sediment depth in meters) + b

	Species	a	b	r^2	concentration (µmol / L)	Depth (m)
5 SL	NO_3^-				45.5[1]	7.5
22 KL	NO_3^-	0.266	37.88	0.65	43.5	22
35 SL	NO_3^-	-0.415	52.84	0.85	45.4	18
53 SL	NO_3^-				46[1]	5
81 SL	NO_3^-				50 ?	
96 SL	NO_3^-	-0.153	51.18	0.38	48.9	15
35 SL	O_2	3.71	0.9029	0.95	65.9	18
69 SL	O_2	2.98	4.48	0.95	204	70

630   [1] Estimated from the values and trend at the core base.

635

640
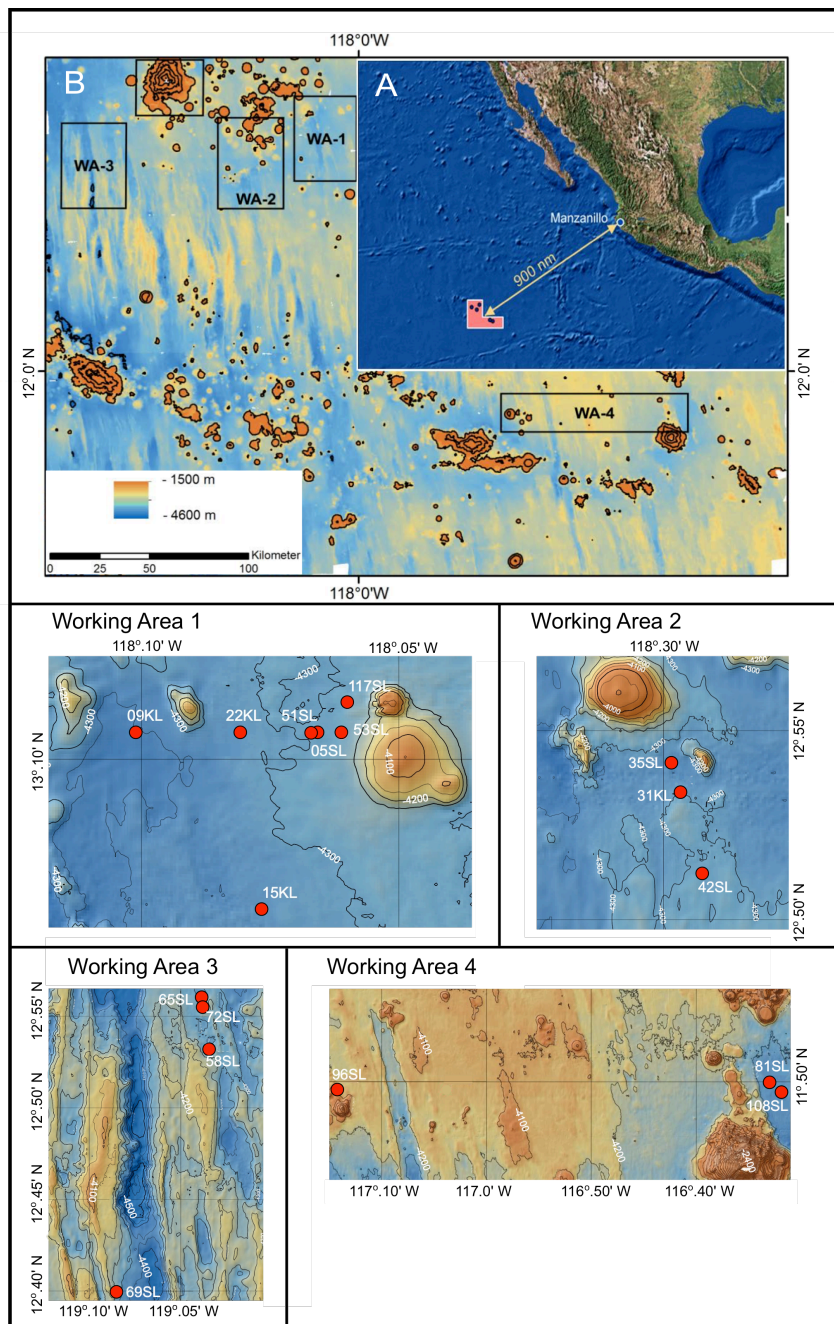
Figure 1: Maps. Top panel A. Geographical setting. B. Bathymetric map of the region of investigation with the four working areas
indicated. Lower four panels, bathymetric maps of the working areas with core locations indicated by red dots.
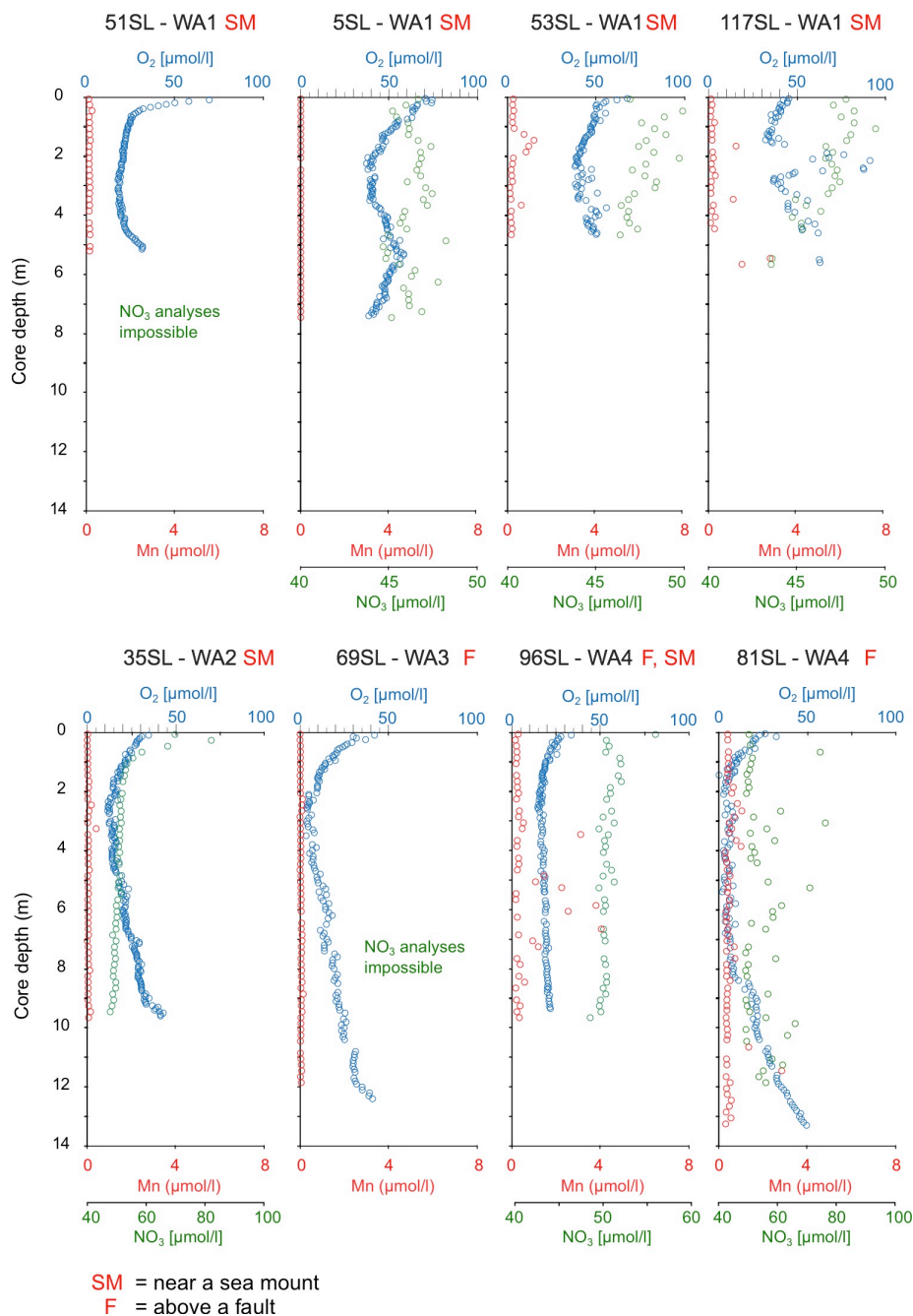
Figure 2: Dissolved oxygen, manganese and nitrate profiles of cores without free porewater Mn²⁺. For all cores, nitrate profiles do not display significant denitrification beyond the uppermost meter (e.g., in 35SL). NB: core 5SL may reflect disequilibrium conditions due to recent slumping. NB: Nitrate increase with depth for 81SL is aberrant as is the absence of free manganese.
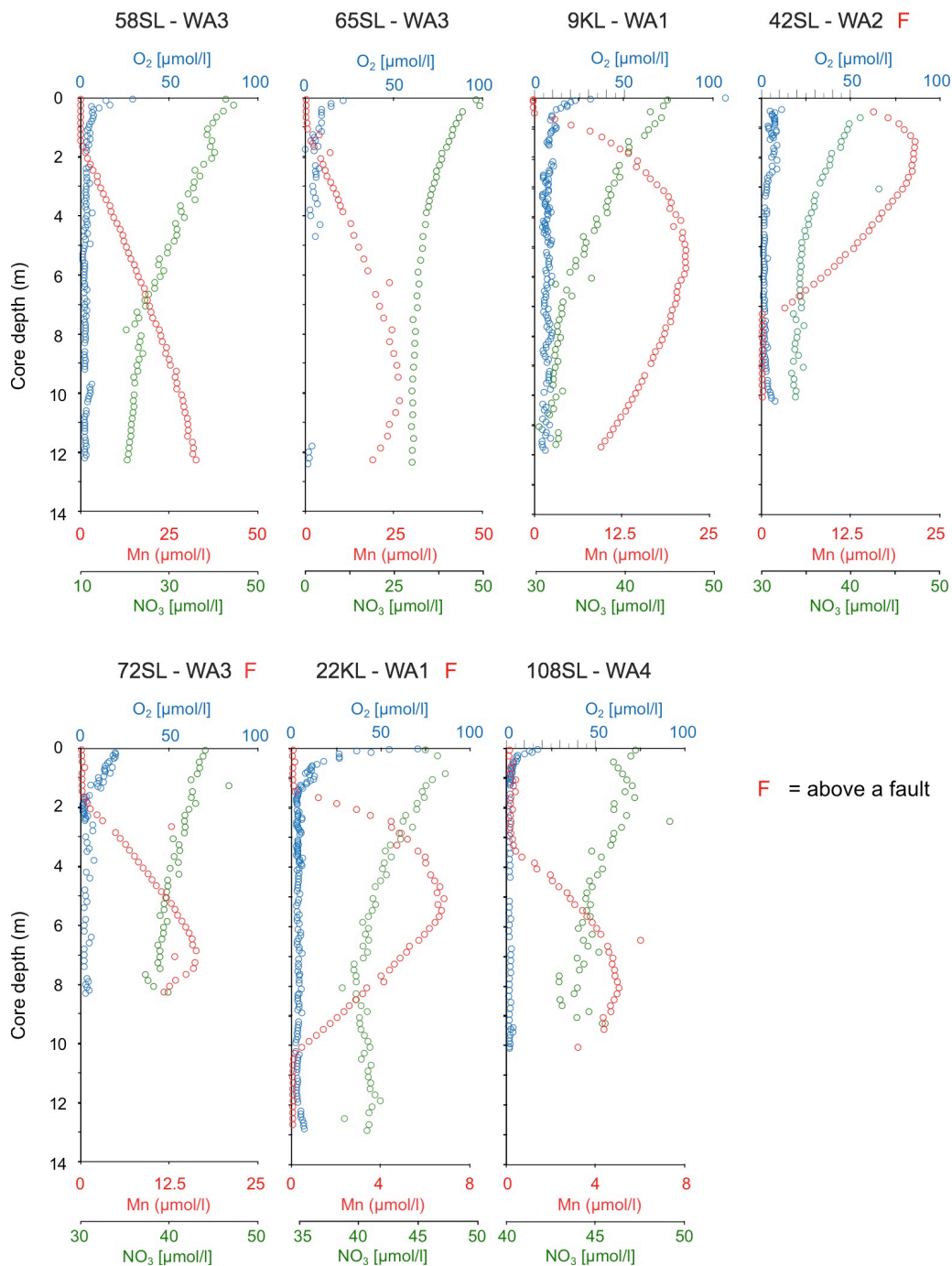
655 **Figure 3: Dissolved oxygen, manganese and nitrate profiles of cores with free porewater manganese in order of maximum manganese concentrations (decreasing minimum nitrate values). For all cores nitrate values reach below the inferred value for basement fluid of 45 µmol/l, suggesting the sediments at these locations are nitrate sinks. Core 22KL illustrates this with a nitrate minimum at 7 m core depth, indicating the depth where denitrification equals the nitrate fluxes from above and below.**

660
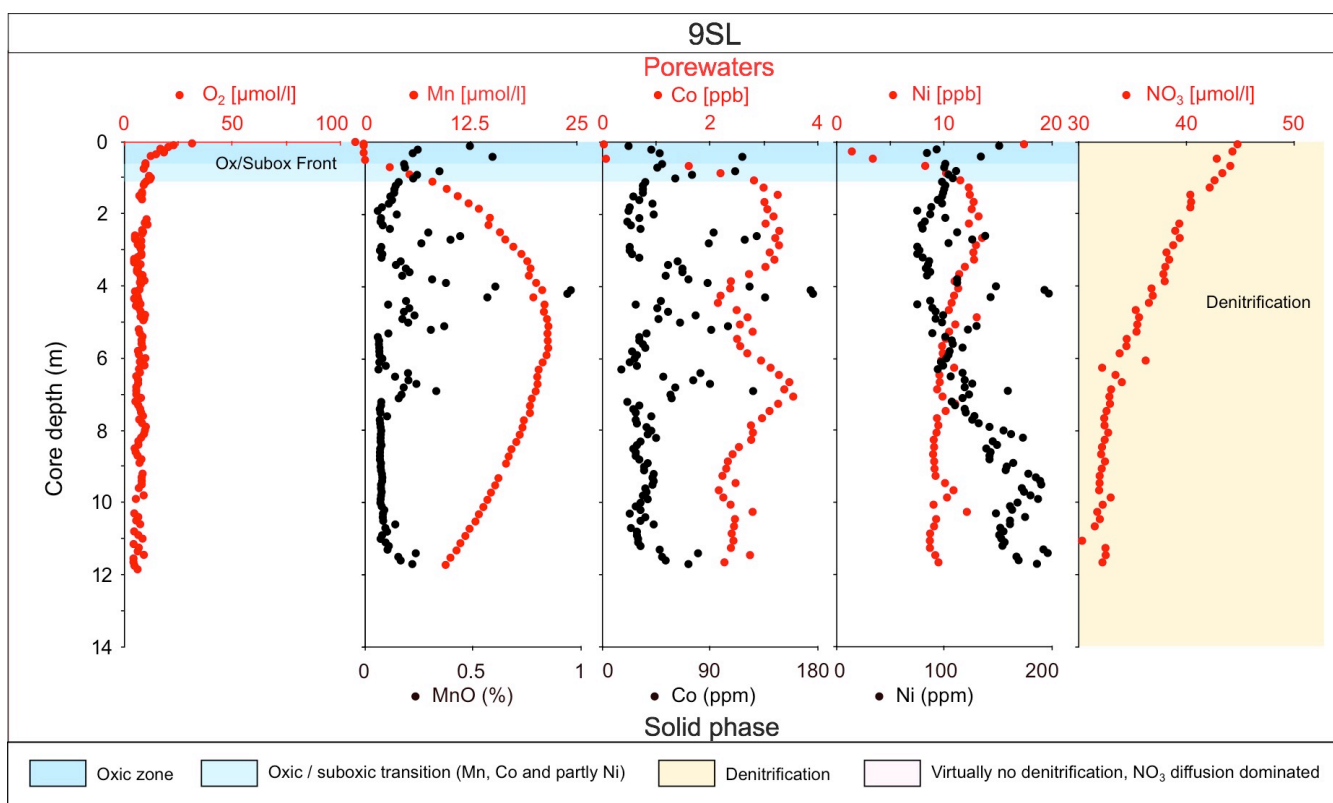
Fig 4a

670

675
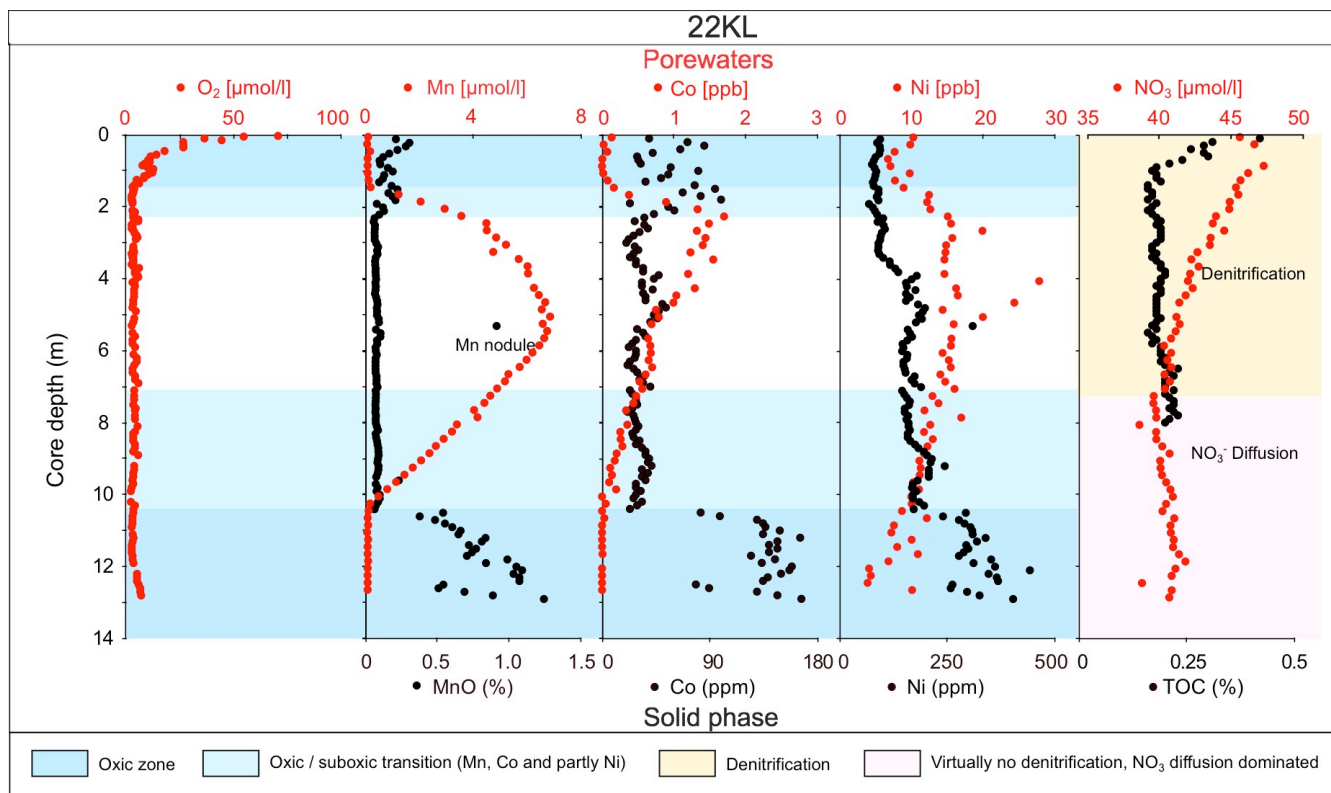
680   **Fig 4b**

685

690
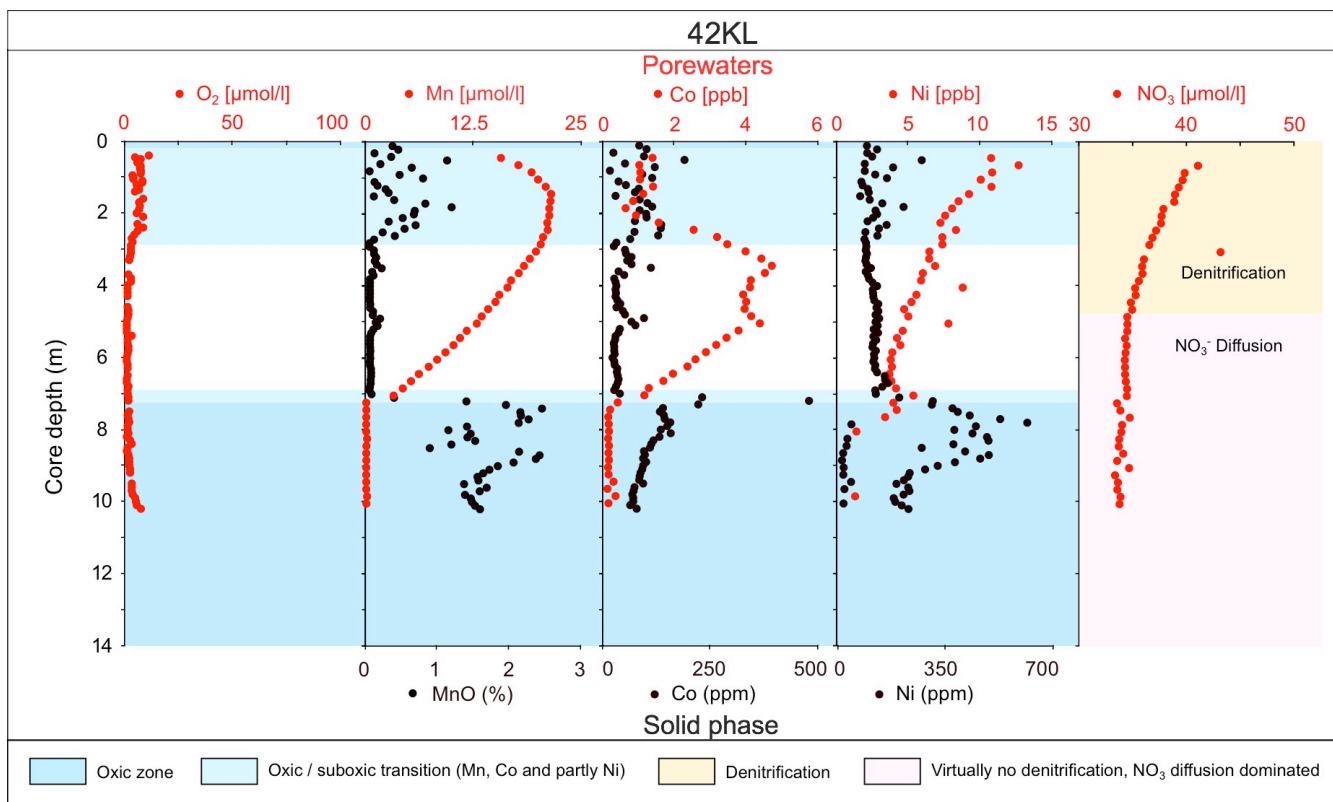
Fig 4c

695

700
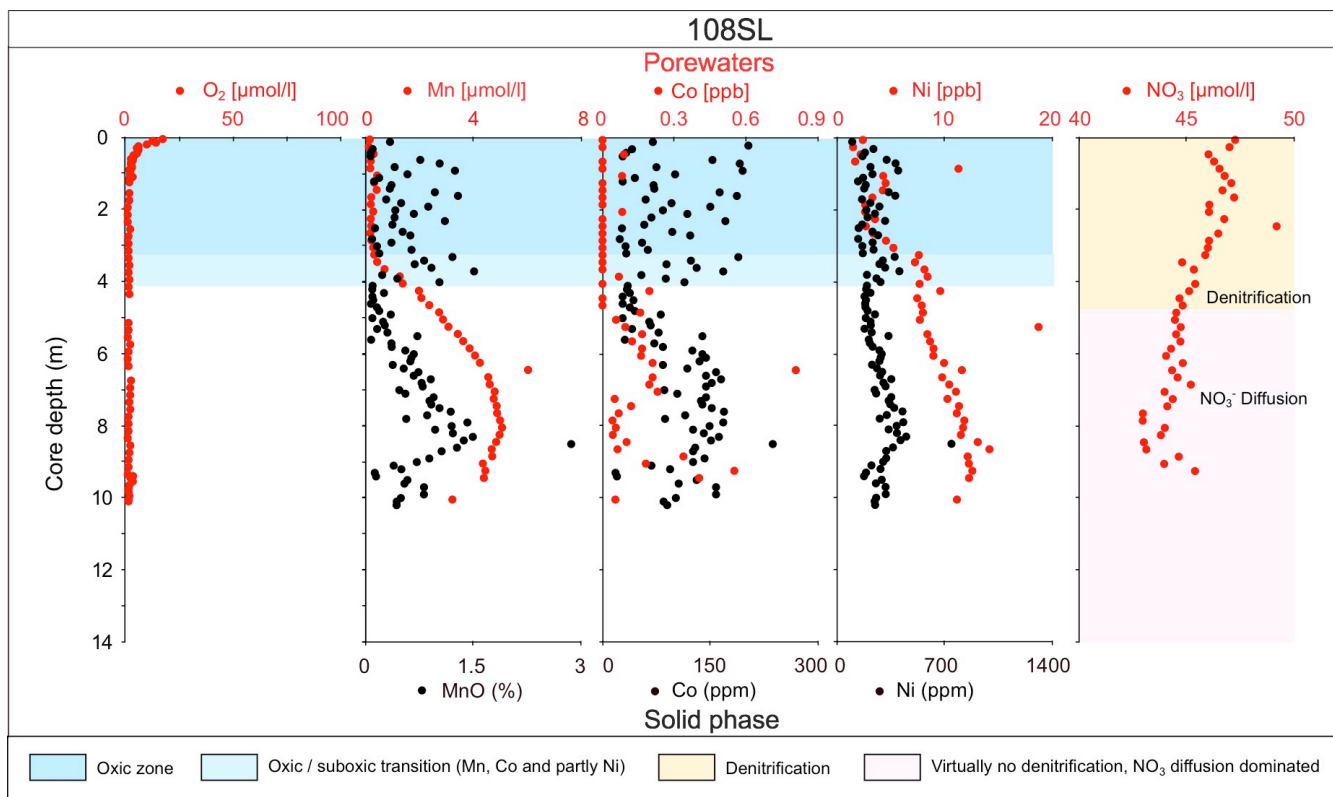
Figure 4a–d: Combined porewater and solid–phase profiles for oxygen, Mn, Co, Ni, and nitrate in the cores with suboxic zones.
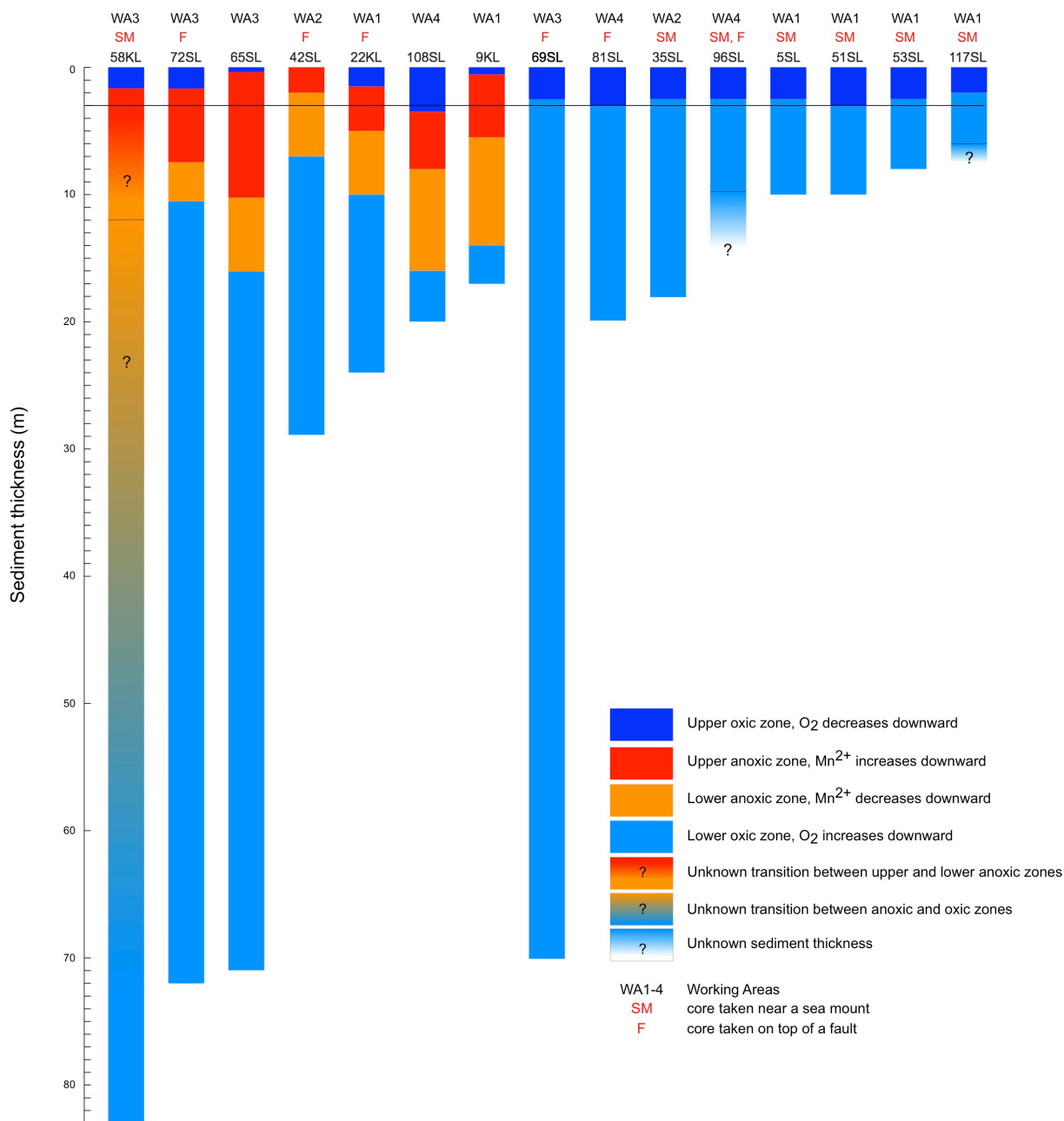
Figure 5: Compilation of oxygenation states of cores for the entire sediment column (sediment surface to basement) taken during RV *Sonne* Cruise SO240. Sediment thickness is based on seismic and parasound data (Kuhn et al., 2015); oxidation state based on core porewater oxygen and manganese concentrations. Note that for the totally oxic cores (blue only) the oxygen minimum (where the downward dark blue, and upward light blue oxygen profiles meet) is always in the upper few meters. The upper oxic/suboxic transition also occurs in the upper few meters. The black line at 3 m depth marks the lower limit of the upper oxic zone for all cores except for 108SL.

730

735
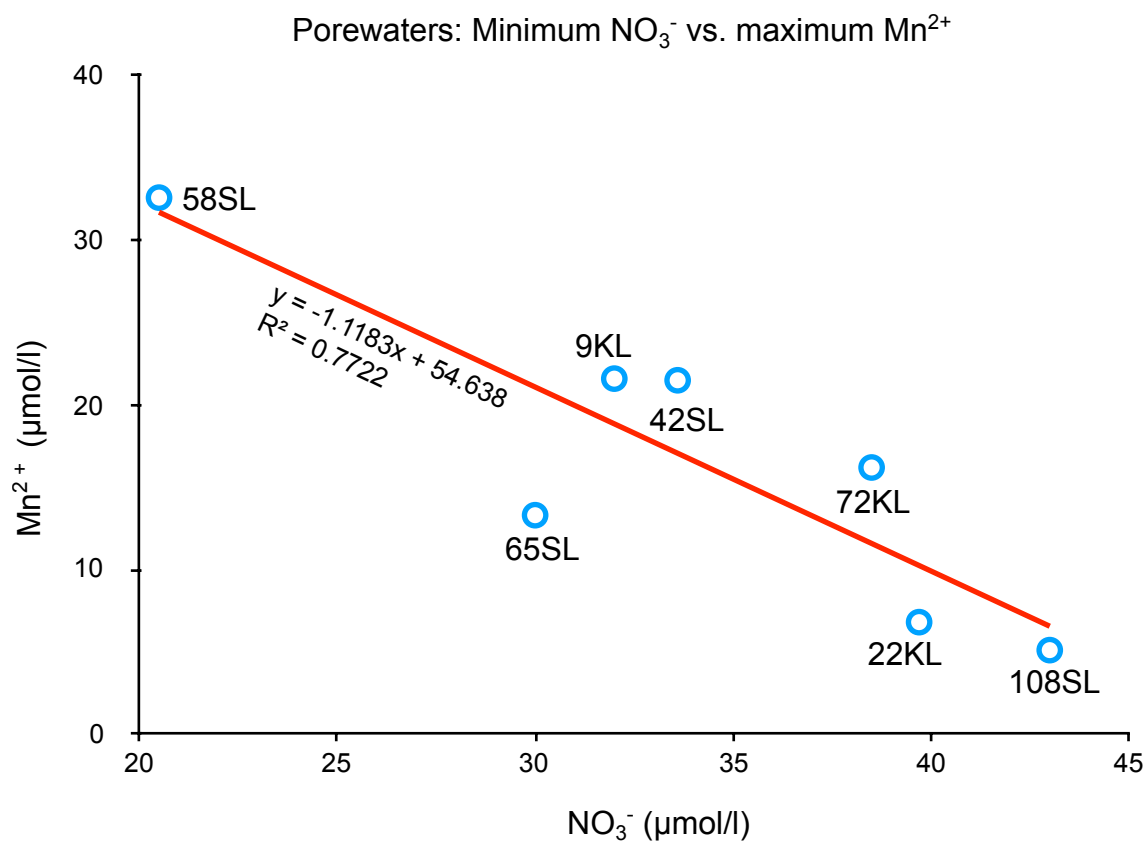
740

Figure 6: Relationship between maximum Mn2+ and minimum NO_3^- concentrations for the cores with a suboxic zone.

745
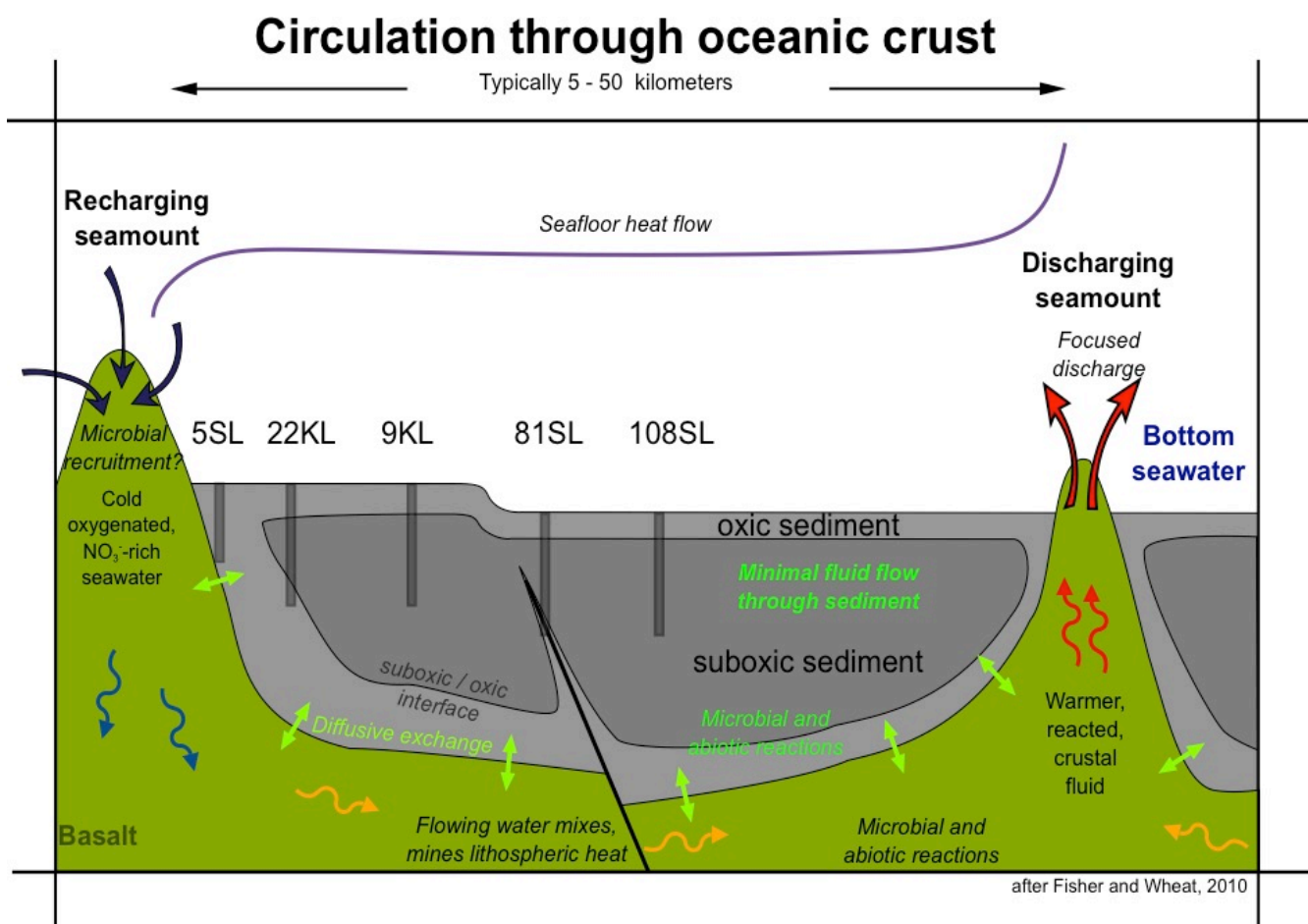
750

Figure 7: Model of fluid circulation in the basaltic basement, diffusive exchange with the sediment and the sediment oxidation state. Note the influence of faults. Representative cores taken during SO240 are placed such that their geochemical profiles match with the model (modified from Fisher and Wheat, 2010).

755
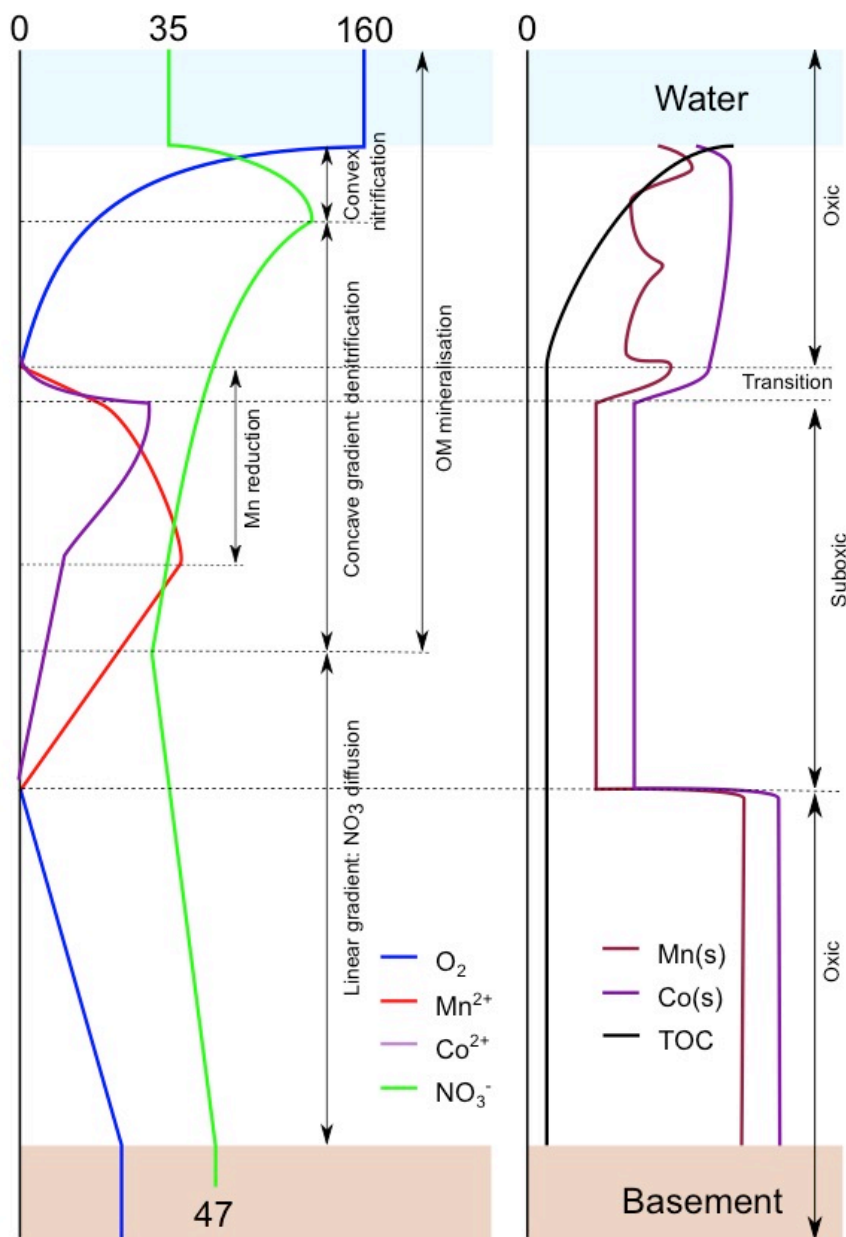
760

Figure 8: Conceptual model summarising the diagenetic processes discussed in this paper as a result of oxygen entering the sediment from the ocean bottom waters and from the oceanic basement. Left panel: porewater profiles, Right panel solid fraction. Numbers refer to concentrations in µmol/L. The model is based on the profiles of inorganic species and TOC in core.